Bremsstrahlung in hot plasmas with partially ionized atoms

M. Lamoureux[1,*] and N. Avdonina[2]
[1]*Laboratoire de Physique Atomique et Nucléaire, Université Pierre et Marie Curie, 4 place Jussieu, 75252 Paris, France*
[2]*Department of Physics and Astronomy, University of Pittsburgh, Pennsylvania 15260*
(Received 27 February 1996; revised manuscript received 19 August 1996)

Analytical bremsstrahlung results are obtained in an ionic radial potential whose screening constant λ_i due to the bound electrons can be parametrized in terms of the atomic number and the degree of ionization. By comparison with exact numerical results published for various incident electron energies E, the precision obtained for the cross sections is discussed in view of determining the energy losses W, and the emissivity coefficients J and total power losses P for Maxwellian plasmas of temperature T. The discrepancy between the Born and Elwert-Born results for these three quantities is explained and the evolution with decreasing ionization from the Coulomb to the neutral case is studied. The relative reduction of the radiation with increasing screening is obtained satisfactorily in the simple approximations. Extrapolations using these reductions and tables of exact W's published for neutral atoms lead to ionic energy losses accurate to within 5%. However W, J, and P can all be determined successfully by direct simple expressions involving E/λ_i^2, $h\nu/\lambda_i^2$, and/or kT/λ_i^2. The precision is at worst 25% and in most cases only a few percent, especially in the range of a few tens of keV. [S1063-651X(97)02201-0]

PACS number(s): 52.25.Nr

I. INTRODUCTION

Bremsstrahlung is an atomic process of importance in hot plasmas both for its dominant contribution to the energy losses [1,2] and for a current temperature diagnostic [3,4]. We recall that the energy loss $W(E)$ for an electron of given energy E is obtained by integrating from zero to one over the fraction $h\nu/E$ of energy radiated. The emissivity coefficient $J(h\nu)$ at the photon energy $h\nu$ is obtained by summation over the free electrons of the plasma, which are assumed here to follow a Maxwellian distribution at temperature T. The total power loss P is the result of the double integration. We will determine W, J, and P for partially ionized ions, taking into account the screening by the bound electrons and neglecting any screening by the free electrons of the plasma. Our treatment is thus restricted to the temperature-density region where the Debye-Hückel screening constant $\lambda_{DH}=[4\pi e^2 N_e/kT]^{1/2}$ is close to zero. We will make direct determinations in the Born and Elwert-Born (EB) approximations by use of a parametric screened radial potential. The precision can be improved by extrapolation from the neutral limit, for which accurate cross sections and W have been published [5]. The main utility of our approach will be for moderately hot plasmas where bremsstrahlung from partially ionized atoms dominates the radiation. On the one hand, at high temperatures most free electrons are very energetic and the Coulomb cross sections (in the Z/r potential) are appropriate, even for the few ions that may not yet be fully stripped. On the other hand, at low temperatures line emission and radiative recombination would dominate. Therefore, the present study mostly deals with temperatures T of a few keV and tens of keV. The plasma will be assumed Maxwellian and optically thin.

In the past W, J, and P have been calculated extensively and exploited on the basis of Coulomb cross sections, sometimes not even at their best level of accuracy. The straightforward estimates W_{Kr}, J_{Kr}, and P_{Kr} based on Kramers (Kr) cross sections most often provide correct orders of magnitude. The more precise results, including for the screened cases, are conveniently expressed by their dimensionless ratios over the Kramers values, i.e., W/W_{Kr}, J/J_{Kr}, and P/P_{Kr}, where the Kramers estimates recalled in Eqs. (13), (19), and (27) are taken in the Z/r potential. The Coulomb results should be applied only to very hot plasmas where all ions are fully stripped. However, in the more general situation where partially ionized atoms are present, the same simulations and interpretations are nearly always adopted, except for very dense plasmas where a few types of average atoms models have been be used [6–8]. In doing this, it has been hoped that the presence of bound electrons around the nucleus does not introduce important modifications. It has also been realized that more precise treatments would be lengthy and that the numerous atomic data needed, in general, are not available or are very difficult to obtain.

The purpose of this paper is to evaluate how misleading the optimism underlying the use of Coulomb results is and to propose easy determinations of ionic radiative losses and emissivities with good accuracy. Several first steps to finding solutions to this problem have been taken recently [9,10]. The interpolation laws presented in Ref. [9] are, unfortunately, of very limited applicability because the parametric ionic potential used is available only in a few cases and because the Coulomb exact data needed are very scarce. In this work, we give a general expression of the screening ionic constant and we find solutions that do not require the knowledge of Coulomb data. We discuss in details the precision of two *ab initio* determinations for wide ranges of energies and we also propose results obtained by extrapola-

*Present address: Laboratoire de Dynamique des Ions, Atomes et Molécules, Case 75, Université Pierre et Marie Curie, 4 place Jussieu, 75252 Paris, France.

tions out of the neutral case. This work also goes beyond Ref. [9] by studying not only the cross sections and W, but also J and P. Moreover, we express the results by formulas that are easy to use and to apply numerically.

Section II deals with the ionic radial potential and the resulting bremsstrahlung cross sections. Analytical cross sections [9] have been obtained in Born and EB approximations from a radial ionic potential depending on the screening parameter λ_i and it was also observed that the ratios of the neutral atom to Coulombic cross sections are obtained from simple models with a good precision, even when the cross sections themselves are not accurate. This fact had been noticed at lower E's with a classical mechanics model [11]. This feature enabled the authors to find fruitful interpolation laws between the neutral atom and Coulomb limits. Applications are limited in practice because of the extreme rarity of precise Coulomb cross sections [12] (data are available for only three Z's and six values of E) and also because only a few λ_i are accessible (only six Z's and a few degrees of ionization). We propose here a convenient parametrization of λ_i in terms of the atomic number Z and the degree of ionization Z_i [see Eq. (2)]. We analyze the validity of the Born and EB cross sections themselves for three atomic numbers and $E=1$–500 keV, in view of the determination of P, W, and J, especially since inaccuracies can be smoothed out in the later integrations. The accurate quantum-mechanical cross sections tabulated for neutral atoms [5] are taken as exact values in the comparison. In the absence of very precise data for the Coulomb case, we use the ones obtained from the recommendations of Pratt and Feng [13]. This discussion on the bremsstrahlung cross sections helps to find appropriate strategies to calculate the radiative losses and the emissivities with good accuracy.

The energy loss $W(E)$ per unit length of path of an electron of energy E is determined in Sec. III. The direct Born (B) and EB estimates are indicated in Eqs. (14) and (15). The constant value of the ratio $W^{\mathrm{EB}}/W^{\mathrm{Born}}$ is accounted for. As for the cross sections themselves, the ratio of the energy losses for neutral atoms over the ones for fully stripped ions is nearly independent of the atomic model used. Interpolation laws between the Coulomb and neutral atom cases would be of little use, unfortunately, again because of the scarcity of precise Coulomb data [12] (only two Z's and three values of E). Very precise evaluations can be obtained instead by extrapolations from energy losses tabulated for the neutral atoms [5], as indicated by Eq. (17a). A quicker and less accurate (better than 25%, however) estimate of W/W_{Kr} is given by Eq. (17b); it involves only Z_i/Z and E/λ_i^2.

Section IV deals with the emissivity coefficients $J(h\nu)$, which are obtained by integrations over an isotropic and Maxwellian distribution at temperature T. Use of the Gauss-Laguerre method [14] of integration is convenient and precise enough. Moreover, it enables one to find the $h\nu/T$ dependence of the ratio $J_{\mathrm{EB}}/J_{\mathrm{Born}}$. For large photon energies or at high temperatures the relativistic Coulomb Gaunt factors have to be used in the Gauss-Laguerre summation and the nonrelativistic results of [15] are not valid. In the lower regime, when screening is important, use of the nonrelativistic EB Gaunt factors of Eqs. (6) and (8) in Eq. (25) leads to satisfactory determinations, accurate to within 10% in general. The J/J_{Kr} result depends on Z_i/Z, $h\nu/T$, and T/λ_i^2.

The determination of the total power loss P/P_{Kr} is presented in Sec. V. The easiest evaluation is through Eq. (28), using W values at the desired accuracy; that is, Eq. (17a) for excellent precision and Eq. (17b) for a precision better than 10%. In last case P/P_{Kr} is a simple function of Z_i/Z and T/λ_i^2.

II. DETERMINATION OF THE BREMSSTRAHLUNG CROSS SECTIONS

Two types of parametric potentials have been proposed in the past to describe the very interior or the interior parts of an atomic system. A potential of the form $rU_1=-Z[1.0+V_{i1}(\lambda r)+V_{i2}(\lambda r)^2+\cdots]$ correctly fits the Hartree-Fock-Slater potential deep inside the atom. Its resourcefulness has been demonstrated for continuum wave functions and phase shifts [16], photoeffect at high energies [17], and internal conversions [18]. Values of λ and V_{ij} have been tabulated for six atoms of Z ranging from 13 to 92 with various degrees of ionization Z_i [19]; they were reproduced in figures, but only for neutral atoms, in a more accessible article [18]. Another kind of parametric potential expresses rU_i by a sum of two Yukawa terms $\exp(-\alpha r)$. It leads to analytical expressions of the electron bremsstrahlung cross sections in the nonrelativistic Born approximation. Such cross sections, involving the Debye screening constant, were used to calculate opacities in dense plasmas [6]. More recently, a potential consisting of a Coulomb tail and a screened core has been used to determine cross sections for isolated free ions [9]. The applications were restricted to ions for which screening values were accessible. In this work, we provide a general determination of the screening constant and we discuss the validity of the cross sections obtained for $E=1$–500 keV.

A. Parametric potential

The radial atomic potential

$$rU_i(r)=-Z_i-(Z-Z_i)\exp(-\lambda_i r) \tag{1}$$

is especially well suited to describe ions of atomic number Z and degree of ionization Z_i. We recall in passing that the Thomas-Fermi model gives $\lambda_0=0.57Z^{1/3}$ for the neutral atom. The screening constant proposed here is better adapted to the interior of the atom, as required by the treatment of bremsstrahlung at moderate energies. We determine it by using tables of λ values [19] that were based on the Hartree-Fock-Slater atomic potential [20]. Figure 1 illustrates the accuracy of our fit $\lambda_0=0.8932\sqrt{Z}a_0^{-1}$. We then establish the relation of λ_i to λ_0 by using the same tables and the $[1-(Z_i/Z)^{n+1}]/[1-Z_i/Z]$ dependence noticed in Ref. [9]. It enables us to establish a very simple dependence of n upon Z. The resulting value of λ_i to be used in Eq. (1) is thus (in a_0^{-1} units; $a_0=1$ a.u.$=0.529\times10^{-10}$ m)

$$\lambda_i^2=0.798Z\,\frac{1-(Z_i/Z)^{n+1}}{1-Z_i/Z}\,a_0^{-2} \quad \text{with} \quad n=Z(\tfrac{1}{3}-0.0020Z). \tag{2}$$

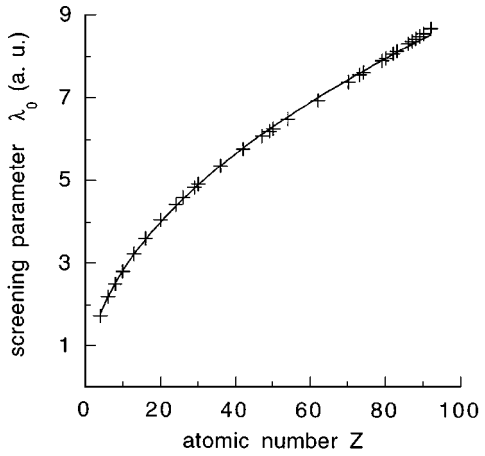

FIG. 1. Screening parameter λ_0 of Eq. (1) in a.u. (a_0^{-1}) for neutral atoms of atomic number Z. Data points are fitted by the curve $0.8932\sqrt{Z}$.

B. Analytical bremsstrahlung cross sections

The main features of electron bremsstrahlung, i.e., the radiation of a photon as an electron is scattered by an atom or ion, can be found in review papers [13]. We are interested in the differential cross section $d\sigma(E,h\nu)/d(h\nu)$, already integrated over the emission angles of the photon and of the electron. The Kramers cross section was obtained in a semiclassical model and amounts to

$$\frac{d\sigma_{\rm Kr}(E,h\nu)}{d(h\nu)}=\frac{Z^2}{h\nu(v/c)^2}\,s_{\rm Kr}\quad\text{with}\quad s_{\rm Kr}=\frac{16\pi}{3\sqrt{3}}\,\alpha_{\rm FS}^3\left(\frac{\hbar}{mc}\right)^2, \tag{3}$$

where c is the speed of light, m the mass of the electron, $\alpha_{\rm FS}$ the fine-structure constant, v the velocity of the incident electron, and $s_{\rm Kr}=5.61\times10^{-31}$ m^2=5.61 mb. In more elaborate calculations or in measurements, the scaling in $h\nu$ and v^2 remains precious to provide correct orders of magnitude. The so-called reduced cross section $s(E,h\nu)$ in Eq. (4) is the quantity tabulated in most published data tables. The dimensionless Gaunt factor is the ratio of any type of cross section, be it experimental or theoretical, over the Kramers cross section

$$\frac{d\sigma(E,h\nu)}{d(h\nu)}=\frac{Z^2}{h\nu(v/c)^2}\,s(E,h\nu)=G(E,h\nu)\,\frac{d\sigma_{\rm Kr}(E,h\nu)}{d(h\nu)}. \tag{4}$$

The most sophisticated quantum-mechanical cross sections in our domain of interest are obtained from the multiple relativistic partial-wave (PW) model [21]. Its quality was confirmed by confrontations with other models in the Coulomb case and by comparisons to very scarce experimental results for neutrals. After a few data points have been published for neutral atoms [21,12] or ions [22], the $s(E,h\nu)$ have been tabulated [5] for all neutral atoms of Z=1–92, with fixed E values ranging from 1 to 2000 keV, and for proportions of energy radiated from 0 up to 100%. Since there are very few experimental results for neutral atoms and none for ions, these PW theoretical data will be used in order to evaluate the quality of our cross-section estimates.

The Born analytical cross sections involve the screening parameter $\lambda_1(Z,Z_i)$ of Eq. (2) and the maximum and minimum momenta transferred in the collision

$$k_\pm=\frac{\sqrt{2mE}\pm\sqrt{2m(E-h\nu)}}{\hbar}. \tag{5}$$

The Gaunt factor for the ion with $\alpha=Z_i/Z$ writes, in the nonrelativistic Born approximation,

$$G_B^i(E,h\nu)=\frac{\sqrt{3}}{2\pi}\left\{\alpha^2\ln\frac{k_+^2}{k_-^2}+[1-\alpha^2]\ln\frac{k_+^2+\lambda_i^2}{k_-^2+\lambda_i^2}+\lambda_i^2[1-\alpha]^2\left[\frac{1}{k_+^2+\lambda_i^2}-\frac{1}{k_-^2+\lambda_i^2}\right]\right\}. \tag{6}$$

While the Gaunt factor depends simply on k_+^2/k_-^2 for the Coulomb case, it depends also on k_+^2/λ_i^2 and k_-^2/λ_i^2 for the screened case.

As it is well known [13], the Elwert factor $\mathcal{E}_F(E,h\nu)$ in Eq. (7) has been introduced in the Coulomb case to improve the cross sections for high proportions $h\nu/E$, where G would unphysically tend to zero otherwise. It involves the quantity β and β' of the incident and of the outgoing electrons, with $\beta=v/c$. In the energy range treated here, we observed that the ratio involving the exponentials is very close to unity. Unless otherwise specified, we will therefore use the more simple and nonrelativistic Elwert factor $\mathcal{E}(E,h\nu)$. The full and simplified Elwert factors are

$$\mathcal{E}_F(E,h\nu)=\left[\frac{\beta}{\beta'}\right]\left[\frac{1-\exp(-2\pi Z\alpha_{\rm FS}/\beta)}{1-\exp(-2\pi Z\alpha_{\rm FS}/\beta')}\right],$$

$$\mathcal{E}(E,h\nu)=\frac{\sqrt{E}}{\sqrt{E-h\nu}}. \tag{7}$$

The Gaunt factor corresponding to the Elwert-Born approximation becomes, in the simple version,

$$G_{\rm EB}^i(E,h\nu)=\frac{\sqrt{E}}{\sqrt{E-h\nu}}\,G_B^i(E,h\nu). \tag{8}$$

At the tip end, we have

$$G_{\rm EB}^i\xrightarrow{h\nu/E\to1}\frac{\sqrt{3}}{2\pi}\left\{\alpha^2+\frac{1-\alpha^2}{1+\dfrac{\lambda_i^2}{k_{\rm ph}^2}}-\frac{\lambda_i^2}{k_{\rm ph}^2}\frac{(1-\alpha)^2}{\left(1+\dfrac{\lambda_i^2}{k_{\rm ph}^2}\right)^2}\right\}, \tag{9}$$

where the photon energy is characterized by $k_{\rm ph}^2=2mh\nu/\hbar^2$. Notice that the screened Gaunt factor is reduced in comparison to the Coulomb value $\sqrt{3}/2\pi$. At the other limit when $E\gg h\nu$, we have

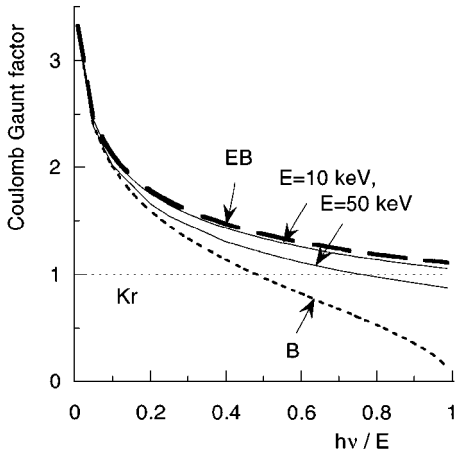

FIG. 2. Gaunt factor for the Coulomb cross section vs the proportion of energy radiated $h\nu/E$. Simple evaluations of Eq. (11) for Kramers (Kr), Born (B), and Elwert-Born (EB) approximations. Also indicated (—) are the relativistic Elwert-Born-Gaunt factors [23] for Ag^{47+} at the incident electron energies $E=10$ and 50 keV.

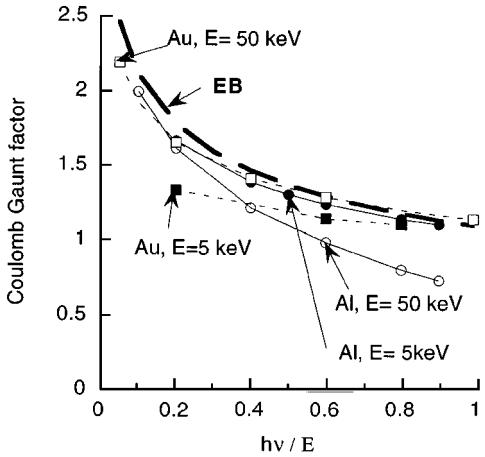

FIG. 3. Coulomb Gaunt factors vs $h\nu/E$. Comparison of the EB (––) simple evaluation of Eq. (11) with elaborate PW data [12] for fully stripped Al (circles) and Au (squares) at $E=5$ and 50 keV.

$$G_{\mathrm{EB}}^{i} \xrightarrow{h\nu/E\to 0} \frac{\sqrt{3}}{2\pi}\{(1+\alpha^2)\ln(4E)-2\alpha^2\ln(h\nu) + (1-\alpha^2)\ln\left(\frac{2m}{\hbar^2\lambda_i^2}\right)-(1-\alpha)^2\}. \tag{10}$$

C. Cross-section results for the Coulomb case

Some typical features recalled for Coulomb bremsstrahlung are helpful to probe the simple approximations. The Kramers-Gaunt factor, the Born-Gaunt factor, and the simplified Elwert-Born-Gaunt factor are

$$G_{\mathrm{Kr}}=1, \quad G_B^{\mathrm{Cb}}=\frac{\sqrt{3}}{\pi}\ln\frac{\sqrt{E}+\sqrt{E-h\nu}}{\sqrt{E}-\sqrt{E-h\nu}},$$

$$G_{\mathrm{EB}}^{\mathrm{Cb}}=\frac{\sqrt{E}}{\sqrt{E-h\nu}}\,G_B^{\mathrm{Cb}}. \tag{11}$$

They are plotted versus the one variable $h\nu/E$ in Fig. 2. The figure also shows two curves obtained for silver by the analytical formula corresponding to the relativistic Elwert-Born approximation [23] [the full expression of the Elwert factor in Eq. (7) is used then]. The conclusion is that the Elwert factor is necessary and that the relativistic effects are negligible at 10 keV but become appreciable at 50 keV.

Figure 3 compares the $G_{\mathrm{EB}}^{\mathrm{Cb}}$ curve to some of the scarce precise PW data points available [12,24]. The $G_{\mathrm{EB}}^{\mathrm{Cb}}$ values are significantly different from the PW values for Al at $E=50$ keV above $h\nu/E=0.5$ and for Au at $E=5$ keV below $h\nu/E=0.4$. In both cases, better Coulomb evaluations are obtained through the recommendations of Pratt and Feng [13], who defined validity domains for various formulas obtained in quantum or in classical mechanics. For Al^{13+} the agreement is reached by the relativistic Elwert-Born formula, leading to a Gaunt factor of 0.72 versus 0.74 for the PW point at $h\nu/E=0.9$. Qualitatively speaking, the Born approximation remains valid for low Z's until lower energies E, and the relativistic effects, of course, are more important at higher E's. A favorable aspect appears in the total cross sections, though it would not in the angular-dependent cross sections. The relativistic effects and the involvement of the higher multipoles have opposite consequences, so that the nonrelativistic Born approximation remains valid until higher E's than expected. For the second case, Au^{79+} at $E=5$ keV, the good estimate is obtained by classical mechanics, giving 1.33 instead of 1.44 for the PW point at $h\nu/E=0.2$. Of course, this improvement of the Coulomb values, though still achieved by use of analytical formulas, is done at the expense of the simplicity of the formulas and, even more important, without allowing any hope for an easy extension to screened cases.

Among the G of Eq. (11), G_{Kr} and G_B^{Cb} are failing at moderate energies, either for not reproducing the steep ascent at small $h\nu/E$ values or for leading to an unreasonable descent at large $h\nu/E$. For E of a few tens of keV, $G_{\mathrm{EB}}^{\mathrm{Cb}}$ is definitively the most satisfying estimate for fully stripped ions. In the energy domains where it starts to fail or if a better precision is needed, the more complicated set of Coulomb expressions [13] is the recommended solution.

Let us make a last remark on the behavior at the tip at high energies. For a given $h\nu/E$ the $G_{\mathrm{PW}}^{\mathrm{Cb}}$ are decreasing with increasing E for relativistic reasons. For example, the values for Al at $h\nu/E=0.9$ are 1.11, 0.74, 0.64, 0.56, and 0.26 for $E=5$, 50, 75, 100, and 500 keV, respectively [12,24]. The $G_{\mathrm{EB}}^{\mathrm{Cb}}$ estimate goes down to $2\sqrt{3}/\pi=1.10$ at the tip and cannot reproduce values lower than that. On the contrary, G_B^{Cb} goes to zero at the tip. It amounts to 0.36 for $h\nu/E=0.9$ and is thus more satisfactory than $G_{\mathrm{EB}}^{\mathrm{Cb}}$; this happens to be a combined positive effect of the neglect of the relativistic effects *per se* and of the omission of the Elwert factor. At high electron energies, G_B^{Cb} thus happens to be of better quality than $G_{\mathrm{EB}}^{\mathrm{Cb}}$.

D. Cross-section results for screened cases at fixed incident electron energy *E*

Some values for Fe and Mo obtained in Born and EB approximations were presented in detail at $E=5$, 10, 50, and

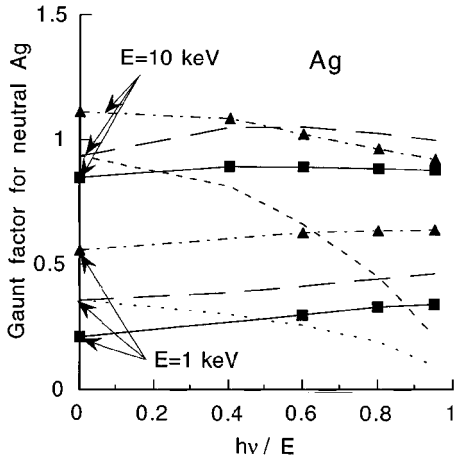

FIG. 4. Gaunt factor for neutral Ag at the incident electron energies of $E=1$ and 10 keV vs $h\nu/E$. ---, Born evaluation of Eq. (6); ––, Elwert-Born evaluation of Eqs. (6) and (8). Triangles and squares are the relativistic numerical Elwert-Born (EBF) and the elaborate PW data points of Ref. [12].

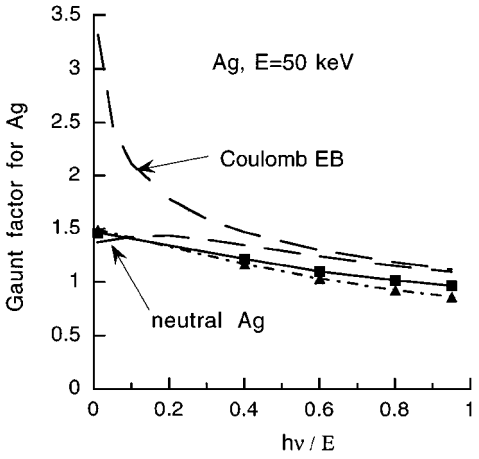

FIG. 5. Same as in Fig. 4, but for $E=50$ keV. ––, EB by Eqs. (6) and (8). Triangles and squares are the EBF and PW data points of Ref. [12]. Also indicated is the EB Coulomb curve of Eq. (11).

100 keV [9]; the full Elwert expression was employed for the EB results. We reproduce very similar values by using Eqs. (2), (6), and (8), which confirms that the parametrization of λ_i and the simplified expression of the Elwert factor are appropriate. The EB values were compared to PW data when available [9] and, for that reason, were restricted to $h\nu/E>0.7$ for ions. For the examples discussed, the agreement was at worst of order 15%, which is, of course, the same for the present EB Gaunt factors. We extend here the discussion of our approximation to lower and to larger E's, where it is expected to be less accurate, and we will also compare the EB estimates to relativistic numerical Elwert-Born results. These additional comparisons will enable us to discuss the validity domains of the EB as well of the Born approximations. The numerical Elwert-Born data quoted below have been determined in the relativistic Elwert-Born form factor model (EBF). The PW and EBF data were obtained from the same relativistic potential [20] and are taken from Ref. [12].

For $Z=47$ at $E=1$ keV, the four models illustrated in Fig. 4 account for the fact that the screening by the bound electrons suppresses the divergence at small $h\nu/E$ typical of the Coulomb case and it significantly diminishes the Gaunt factors in comparison to $G_{\mathrm{Kr}}=1$. The EBF curve lies about twice as high as the PW curve, and this discrepancy is due only to the shortcomings of Born approximation itself, as both models are relativistic and use the same numerical potential. Our EB curve happens to be relatively closer to the PW curve, but is significantly lower than the EBF curve. At such relatively low energies, the discrepancy between the EB and EBF estimates cannot be due to relativistic effects and therefore comes only from a bad description of the potential by our parametrization in the relatively exterior radial region of interest. These two conclusions are confirmed by the fact that the curve [25] obtained in a simple classical mechanics model and not given here is nearly superposed to the exact PW curve when starting from the numerical potential, while our parametrized potential leads in the same model to a curve that lies too low (the values, not plotted here, are 0.10 at the soft end and 0.23 at the tip). The significative distances selected by the classical mechanics approach are, respectively, $0.39a_0$ and $0.37a_0$ at the soft end and at the tip. The radial range involved in Born approximations is roughly given by $1/k_{\pm}$ and is thus estimated to $0.053a_0-233a_0$ at the soft end and $0.11a_0$ at the tip. The parametrization of Eq. (1) is appropriate for $r\ll 1/\lambda_0$, that is, $r<0.163a_0$ for neutral Ag. This is a reason why neither the classical mechanics method nor the Elwert-Born approximation—together with the fact that Elwert-Born approximation is not valid at these energies for Ag anyway—can work when using the parametrized potential of Eqs. (1) and (2). This obstacle disappears, of course, with increasing E's. At $E=5$ or 10 keV, the EBF and EB curves are very similar. Together with the classical mechanics curve (not plotted here), they come close to the PW curve.

Examples are given in Fig. 4 for $E=10$ keV and in Fig. 5 for $E=50$ keV. At 50 keV, the EB, EBF, and PW curves are very close to each other. As expected, the use of the classical mechanics approach has become out of the question. In the energy range $E=1$–500 keV, it never happens that the simple classical mechanics approach using our parametrized potential is doing significantly better than the present EB approximation. Since the Born or EB methods are, by nature, better suited to energies greater than a few tens of keV, only these two models will be kept under scrutiny. The classical mechanics approaches should be reserved to the lower energies and another type of parametrized potential should then be used.

Looking again at Fig. 5, we see that even at $E=50$ keV, the screened case remains significantly different from the Coulomb case until about $h\nu/E=0.2$. At still higher energies such as $E=180$ keV, the agreement of the EB with the EBF values starts to deteriorate. At $E=500$ keV, as shown in Fig. 6, the EB approximation is doing badly except at the soft end. Above $h\nu/E>0.3$, the screened and Coulomb EB results are very similar, and both fail to reproduce the drop with increasing photon energies. The EB approximation improved by using the full expression of the Gaunt factor in Eq. (7) leads to only slightly better results. The EBF and the PW points are very similar to each other over the whole spectrum; as soon as above $h\nu/E=0.1$ they become very similar

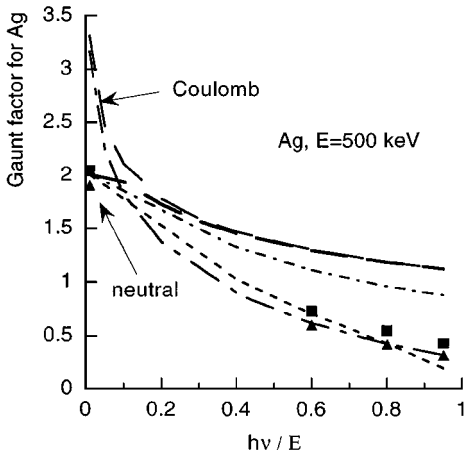

FIG. 6. Gaunt factor for neutral Ag at the incident electron energy of $E=500$ keV vs $h\nu/E$. ---, Born evaluation of Eq. (6); −−−, Elwert-Born evaluation by Eqs. (6) and (8); -·-, Elwert-Born evaluation with use of the full Elwert factor in Eq. (7). Triangles and squares are the numerical relativistic Elwert-Born (EBF) and the elaborate PW data points of Ref. [12]. Also indicated are two Coulomb curves: −−−, Elwert-Born evaluation of Eq. (11); −·−, relativistic Elwert-Born evaluation [23].

to the relativistic Coulomb-Elwert-Born results. As we had noticed for the Coulomb cases relatively to the tip region, the Born approximation happens to be more efficient than the EB approximation. In fact, at $E=500$ keV, the nonrelativistic Born approximation is much more satisfactory than the nonrelativistic Elwert-Born approximation.

E. Cross-section results at fixed photon energies

Since the emissivity coefficients $J(h\nu)$ are calculated from cross sections at a given $h\nu$, it is interesting to consider Gaunt factors in the representation versus E. Figure 7 is a companion to Fig. 2, $h\nu$ being now constant and equal to 10 keV and E varying from 10 to 200 keV. The relativistic effects become appreciable with increasing E's. On the contrary, the discard of the Elwert factor would introduce a large error for small values of $E/h\nu$. Figure 8 shows results for silver ions. Notice that $G(E,h\nu)$ is roughly linear in $\ln(E)$. This is consistent with Eq. (10) and the slopes are, in fact, around $\sqrt{3}/2\pi$ for the neutral and twice more for the Coulomb case.

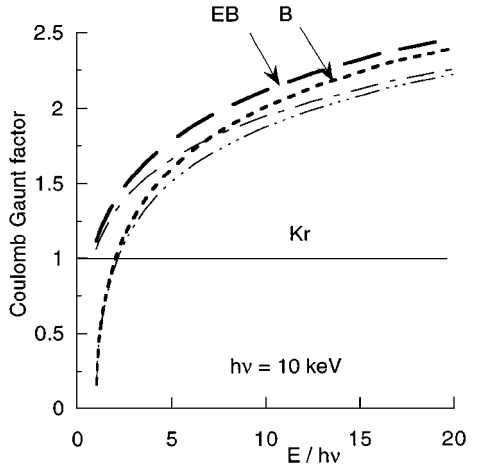

FIG. 7. Gaunt factor for the Coulomb cross section vs $E/h\nu$. Simple evaluations of Eq. (11) for Kramers, Born, and Elwert-Born approximations. Also indicated are the relativistic Born [23] (−−−−−) and Elwert-Born [23] values (−−−) for Ag^{47+} at $h\nu=10$ keV.

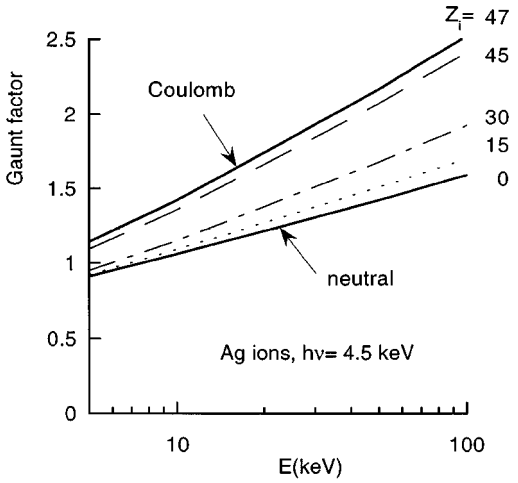

FIG. 8. Gaunt factors for various degrees of ionization of Ag in the Elwert-Born approximation of Eqs. (6) and (8) at $h\nu=4.5$ keV.

III. ENERGY LOSS PER ELECTRON

A. Determination of the energy loss

The energy $W(E)$ radiated by an electron of energy E, per unit length of path and for one ion per unit volume, is given by

$$W(E)=\int_0^E h\nu\,\frac{d\sigma(E,h\nu)}{d(h\nu)}\,d(h\nu),$$

$$\frac{W(E)}{W_{\rm Kr}(E)}=\int_0^1 G(E,h\nu)d\,\frac{h\nu}{E}. \tag{12}$$

In the Coulomb case, the three simplest approaches of Eq. (11) lead to constant values [(dimension)=(energy)×(surface)]

$$W_{\rm Kr}=Z^2\,\frac{8\pi}{3\sqrt{3}}\,\frac{\alpha_{\rm FS}^3\hbar^2}{m},\quad \frac{W_B^{\rm Cb}}{W_{\rm Kr}}=\frac{2\sqrt{3}}{\pi},\quad \frac{W_{\rm EB}^{\rm Cb}}{W_{\rm Kr}}=\frac{2\sqrt{3}}{\pi}\,2\,\ln 2, \tag{13}$$

with $W_{\rm Kr}=1.88\times10^{-6}$ (in a.u.)$=2.29\times10^{-44}$ (in SI units). $W_{\rm Kr}$ and $W_B^{\rm Cb}$ differ only by 10% though the corresponding Gaunt factors are quite different [see Eq. (11) and Fig. 2]. This is due to compensation effects in the course of the integration. It should not be concluded that any other and more elaborate model would also lead to a similar value. Certainly the choice of the method matters less to $W(E)$ than to the Gaunt factors at some critical $h\nu/E$, but it can still play an important role. Here, for example, $W_{\rm EB}^{\rm Cb}$ is bigger by around 50 %. This larger value is a more realistic estimate at moderate E's, as shown in Figs. 2 and 3.

For the screened cases the energy losses have been calculated from the Born and EB Gaunt factors of Eqs. (5), (6),

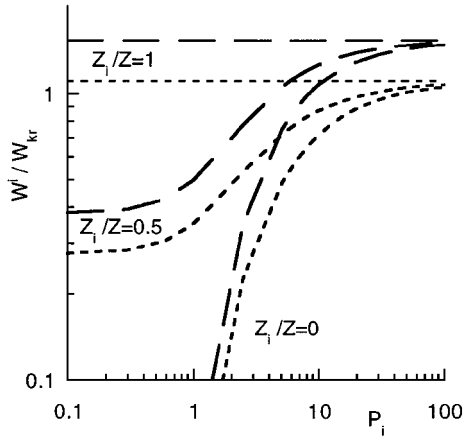

FIG. 9. Energy losses for Ag ions vs P_i as obtained in the Born (---) and EB (––) approximations by Eqs. (14) and (15).

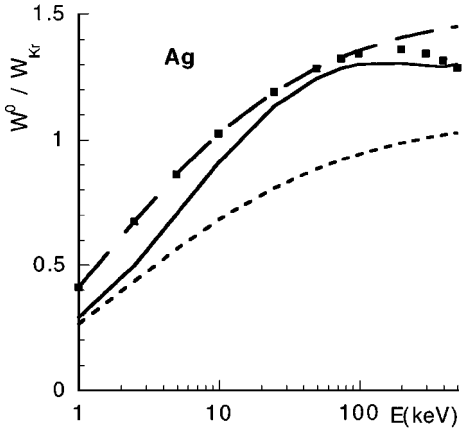

FIG. 10. Energy losses for neutral Ag vs electron energy E. Born (---) and Elwert-Born approximations (––) by Eqs. (14) and (15) and squares from the improved EB approximation by using the Elwert factor $[1-\exp(-2\pi Z\alpha_{\rm FS}/\beta]\ \sqrt{1-h\nu/E}$. The solid line is from the PW elaborate model [5,12].

and (8). For the ion of $\alpha=Z_i/Z$, the dimensionless quantities (which could be called the Gaunt factors relative to the energy losses) are, respectively, in the Born [9] and EB models;

$$\frac{W_B^i(P_i)}{W_{\rm Kr}}=\frac{2\sqrt{3}}{\pi}\left[1+2\,\frac{1-\alpha}{P_i^2}\,\ln(1+P_i^2)-\frac{(1-\alpha)(3+\alpha)}{P_i}\,\arctan P_1\right], \tag{14}$$

$$\frac{W_{\rm EB}^i(P_i)}{W_{\rm Kr}}=\frac{2\sqrt{3}}{\pi}\,2\,\ln 2\left[\alpha^2+\frac{1-\alpha^2}{2\,\ln 2}\,\ln\left(\frac{1+P_i^2}{1+P_i^2/4}\right)+\frac{(1-\alpha)(3+\alpha)}{2\,\ln 2 P_i}\left(\arctan P_i-2\,\arctan\frac{P_i}{2}\right)\right], \tag{15}$$

with the dimensionless variable $P_i=2\sqrt{2mE}/\hbar\lambda_i$, λ_i given by Eq. (2), and E for the incident electron energy.

B. Results of energy losses

Results are plotted in Fig. 9 for $\alpha=Z_i/Z=0$, 0.5, and 1. At large and small values of P, the ordinates go over respectively to the Coulomb Born and EB values given in Eq. (13) or to α^2 times these Coulomb limits. Equations (14) and (15) enable us to treat the transition region. At any given P value, when the electron energy is E for the neutral atom, it is $(1-\alpha)/(1-\alpha^{n+1})\ E$ for the ion, according to Eq. (2).

Results are plotted in Figs. 10 and 11 for a few neutral atoms and for $E=1$–500 keV. They are compared to PW quantum-mechanical tabulated data, the $W_{\rm PW}^0/W_{\rm Kr}$ values being obtained by dividing the last column of the tables [5] upon 4.837. The PW curves are comprised between the Born and EB curves. The energy losses for Ag in Fig. 10 can be discussed by looking at the $G(E,h\nu)$ of Figs. 4–6. At small E, the result of the integration in Eq. (12) ends up being closer to the PW exact values when using Born instead of EB cross sections, as predictable from Fig. 4 for $E=1$ keV. This is a fortunate composite effect that use of the parametric potential and of the Elwert-Born approximation are inappropriate at that energy, as already pointed at in Sec. II D. At higher but still moderate energies, $W_{\rm EB}$ becomes very satisfying, and this on a sound basis. At high E's, the EB method starts to overestimate the energy loss, which could be due to the use of the simplified Elwert factor of Eq. (7). The analytical feasibility in Eq. (12) is maintained and the quality of the $W_{\rm EB}^0$ values slightly improved by using the nearly complete expression $\mathcal{E}(E,h\nu)$ $[1-\exp(-2\pi Z\alpha_{\rm FS}/\beta]$ instead of just $\mathcal{E}(E,h\nu)$. The energy losses for Al and Au in Fig. 11 confirm these conclusions, but the limit energies between which the EB approximation is the better choice are shifted. At lower Z's, the Elwert-Born approximation is known to be valid until lower energies; it is very satisfactory for Al already at $E=1$ keV. With increasing E's, the fact to use a more or less complete form of the Elwert factor matters significantly because Z is low. At $E=10$ keV the $W_{\rm EB}^0[1-\exp(-2\pi Z\alpha_{\rm FS}/\beta)]$ is already an advisable solution. Above around 100 keV, this is not a good enough improvement. G_B^0 has become a better value for reasons indicated in Sec. II D and hence W_B^0 is also a better choice. On the contrary, for the heavier atom Au, it is only above around 15 keV that $W_{\rm EB}^0$ becomes the better choice; it is still the appropriate choice at $E=500$ keV.

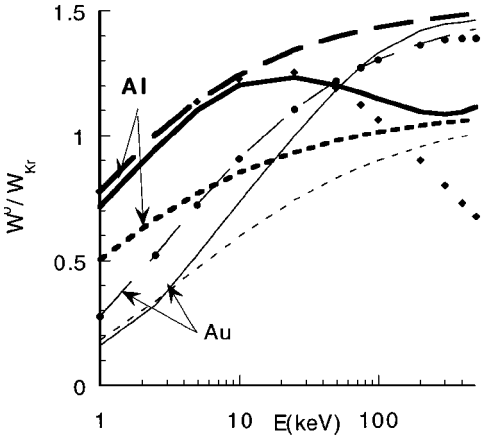

FIG. 11. Same as Fig. 10, but for neutral Al and Au.

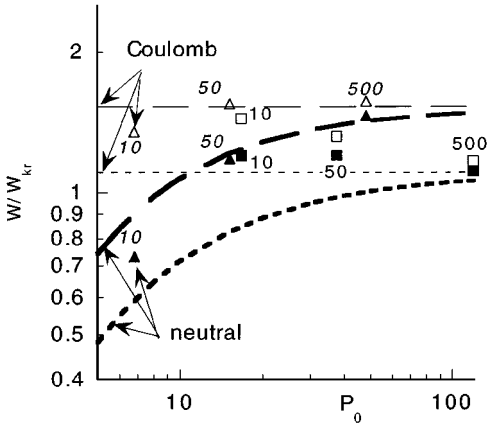

FIG. 12. Comparison of energy losses in the neutral and Coulomb cases vs P_0. Born (---) and Elwert-Born approximations (––) by Eqs. (14) and (15). Full squares and triangles are elaborate PW results [5] for neutral Al and Au and empty squares and triangles are the corresponding results [12] for the Coulomb case, for various values of E in keV.

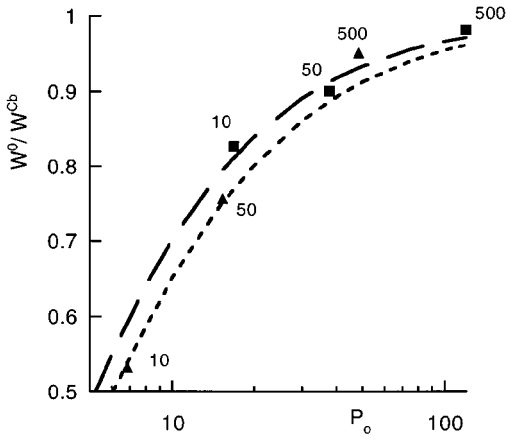

FIG. 13. Ratios of the neutral atom to Coulombic energy losses. Same notations as in Fig. 12, with squares for Al and triangles for Au.

In conclusion, the Born approximation happens to be the better choice either at small or at large energies, whereas the Elwert-Born approximation is very satisfactory at intermediate E's. If we do not want to set Z-dependent limits, it is safe, though restrictive, to say that for these neutral atoms the EB approximation is satisfactory within a precision better than 15% between $E=20$ and 200 keV. This is an excellent accuracy in view of the simplicity of Eq. (15).

C. Discussion in relation with the Coulomb results

In order to improve this already satisfying precision by using interpolation or extrapolation laws involving the Coulomb results, it is necessary to discuss the various Coulomb estimates. Figure 12 and Table I contain the very few quantum-mechanical $W^{\rm Cb}_{\rm PW}$ published [12]. For these six data points, we show again the corresponding neutral $W^0_{\rm PW}$ [5]. Unlike the Born and EB evaluations, the exact estimates depend not only on P_0 but also on Z. Figure 12 and Table I confirm for the neutral atoms and shows for the Coulomb case that the EB approximation is better at moderate P values. The Born approximation becomes more satisfactory at small P's, especially for high Z's, it is again more satisfactory at high P's especially for small Z's.

Figures 9 and 12 also point out that the ratio $W_{\rm EB}/W_B$ is nearly independent of P. At high P values, the ratio goes over to the Coulomb limit, i.e. to 1.39 according to Eq. (13). At small P's, as found for small E's, the $G_{\rm EB}(h\nu/E)$ curves are flat (see Fig. 4). In that situation, G_B is roughly equal to a constant value multiplied by $\sqrt{1-h\nu/E}$ according to Eq. (8). After the integration over $h\nu/E$ in Eq. (12) is done, we obtain $W_{\rm EB}/W_B=1.5$. In the intermediate cases where the $G(E,h\nu)$ is comprised between a Coulomb curve and a flat curve, we thus expect that $W_{\rm EB}/W_B$ amounts to 1.39–1.5 for any ion or energy in our domain of interest. This is indeed what is observed in Figs. 9 and 12. Since $W^{\rm Cb}_{\rm EB}$ and $W^{\rm Cb}_B$ are constant values, it demonstrates at the same time that $W^i_B/W^{\rm Cb}_B$ and $W^i_{\rm EB}/W^{\rm Cb}_{\rm EB}$ are always similar to each other within around 8%, as written down in Eq. (16).

Table I and Figs. 12 and 13 concentrate on comparing the present Born and EB energy loss results to the corresponding PW values, for the limit cases $Z_i/Z=0$ and 1. They deal in details with the Al and Au cases, with E going from 10 to 500 keV. The $W_{\rm EB}$ and W_B are usually obtained with a precision better than 30%. This good agreement is possible, though some of bremsstrahlung cross sections involved may be wrong by as much as 50%. This happens because of the cancellation effects that are produced in the integration over $h\nu/E$. The precision with which the ratios $W^0_{\rm EB}/W^{\rm Cb}_{\rm EB}$ and $W^0_B/W^{\rm Cb}_B$ are obtained is also usually much better than the precision with which any of these four W's is obtained. The case corresponding to Al at $E=50$ keV is particularly illustrative to that respect. Figure 13 and the last two columns in

TABLE I. Relative precision (in %) of the energy losses obtained in the Born (B) and Elwert-Born (EB) approximations from Eqs. (14) and (15) in comparison with the more accurate PW data [5,12]. W^0 and $W^{\rm Cb}$ are the energy losses for the neutral and Coulomb cases relative to Au or Al. The incident electron energy E is in keV and the dimensionless quantity $P_0=2\sqrt{2mE}/\hbar\lambda_0$. The Coulomb data PF correspond to use of the Pratt-Feng recommendations for the cross sections [13].

Atom	P_0	E	$W^\circ\vert_B$	$W^\circ\vert_{\rm EB}$	$W^{\rm Cb}\vert_B$	$W^{\rm Cb}\vert_{\rm EB}$	$W^{\rm Cb}\vert_{\rm FP}$	$W^\circ/W^{\rm Cb}\vert_B$	$W^\circ/W^{\rm Cb}\vert_{\rm EB}$
Au	6.83	10	−18	24	−18	13	−1.5	−0.4	9.4
Au	15.3	50	−30	3	−29	−1	−7.5	−1.4	4.5
Al	*16.8*	*10*	*−41*	*3*	*−23*	*6.1*	*0.7*	*−7*	*−2*
Al	*37.5*	*50*	*−18*	*16*	*−16*	*16*	*−7.0*	*−2*	*0.3*
Au	48.3	500	−31	−3	−30	−2.5	−2.5	−2.5	0.1
Al	*119*	*500*	*−4*	*34*	*−3.7*	*31*	*−24.0*	*1*	*2*

Table I confirm that the ratios W^0/W^{Cb} are very similar in the Born and EB models and also show that they are very similar to the more exact PW estimates

$$\frac{W^i_{\mathrm{EB}}(E)}{W^i_B(E)} \cong 1.39-1.5, \quad \frac{W^0_B(E)}{W^{\mathrm{Cb}}_B} \cong \frac{W^0_{\mathrm{EB}}(E)}{W^{\mathrm{Cb}}_{\mathrm{EB}}} \cong \frac{W^0_{\mathrm{PW}}(E)}{W^{\mathrm{Cb}}_{\mathrm{PW}}(E)}. \tag{16}$$

The ratio W^0/W^{Cb} is better reproduced in the EB model at moderate P values and better in the Born model at extreme P values. If one desires a solution that is P independent, it is as a whole safer to use the Born model, the precision being then better than 7% over the whole P range. The equality of W^0_B/W^{Cb}_B and $W^0_{\mathrm{PW}}/W^{\mathrm{Cb}}_{\mathrm{PW}}$ had been noticed earlier [9], but without any discussion and by using anterior less precise W^0_{PW} [12]. The half sum of the Born and EB ratios is always exact within 4.5% for these examples illustrated in Table I.

D. Recommendation for the evaluation of precise ionic energy losses

The possibility offered by Eq. (16) is to extrapolate the ionic energy loss from the fully stripped value by $W^i(E) = W^{\mathrm{Cb}}_{\mathrm{PW}}(E)[W^i_B(E)/W^{\mathrm{Cb}}_B]$. An interpolation method was suggested [9] between the Coulomb and the screened cases. The practical drawback is the shortage of $W^{\mathrm{Cb}}_{\mathrm{PW}}(E)$ published, in fact only six points. So to get precise Coulomb values, we started from the cross sections recommended by Pratt and Feng [13] and already used in Sec. II C. The $W^{\mathrm{Cb}}_{\mathrm{PF}}$ results are showed in Table I. The agreement with $W^{\mathrm{Cb}}_{\mathrm{PW}}$ is improved in comparison to both the Born and EB models only for two of the six cases available; it remains as high as 7% for Al and Au at $E=50$ keV. Considering that uncertainty and also the one on the ratios $W^i(E)/W^{\mathrm{Cb}}(E)$, we cannot expect to improve the precision of the ionic estimates to much better than 10%. This is hardly an improvement over what is most often achieved by the direct W^i_{EB} or W^i_B estimates.

The other and better possibility is to base the determination of the ionic energy loss on the exact neutral PW energy losses W^0_{PW}. The $W^0_{\mathrm{PW}}(E)$ needed is extrapolated from tabulated values that are densely enough spaced [5]. We obtain the ionic energy loss with a precision of better than around 4.5% by the formula

$$W^i(E) \cong \frac{W^0_{\mathrm{PW}}(E)}{2}\left[\frac{W^i_B(E)}{W^0_B(E)} + \frac{W^i_{\mathrm{EB}}(E)}{W^0_{\mathrm{EB}}(E)}\right], \tag{17a}$$

where W_B and W_{EB} are given by Eqs. (14) and (15).

We recall that if a precision of around 15% is sufficient, W^i_B and W^i_{EB} themselves are a quicker determination, the first one for small and large values of E, the second one for moderate P values. A quick look at the agreement of W^0_B and W^0_{EB} with W^0_{PW} for the energy considered may be a way to decide which approach is better. Finally, a less precise (not worse than 25%, however, and usually much better) but simpler approach is to take the half sum of the Born and EB estimates, which leads to

$$\frac{W^i}{W_{\mathrm{Kr}}} = \frac{2\sqrt{3}}{\pi}\left[\frac{1}{2} + \alpha^2 \ln 2 + (1-\alpha)\left\{\frac{\ln(1+P_i^2)}{P_i^2} + \frac{1+\alpha}{2}\ln\left(\frac{1+P_i^2}{1+P_i^2/4}\right) - \frac{3+\alpha}{P_i}\arctan\frac{P_i}{2}\right\}\right]. \tag{17b}$$

IV. EMISSIVITY COEFFICIENT AND SPECTRUM IN A MAXWELLIAN PLASMA

A. Determination of the emissisivity coefficient

The bremsstrahlung emission in the plasma is due to the collisions of the free electron population energetically partitioned on a distribution function $f(E)$ normalized by $\int_0^\infty f(E)dE=1$. Let us call $N(h\nu)$ the number of photons emitted per second and per unit of photon energy range in a plasma at unit electron and ion densities. By definition the emissivity coefficient [(dimension)=(volume)/(time)] is

$$J(h\nu) = h\nu N(h\nu) = h\nu \int_{h\nu}^{\infty} \frac{d\sigma(E,h\nu)}{d(h\nu)}\, v\, f(E)dE, \tag{18}$$

v being the velocity of the incident electron in the bremsstrahlung collision. Consequences of a possible non-Maxwellian character on the spectra have been studied experimentally and theoretically for various cases mentioned, for example, in Ref. [26]. We concentrate here on the influence of a not complete ionization on the bremsstrahlung emission and consider only Maxwellian plasmas. When Kramers cross sections are used the Maxwellian emissivity coefficient (for the 4π s and the two modes of polarization) takes the simple expression

$$J_{\mathrm{Kr}}(h\nu) = \frac{1}{2^{1.5}3^{1.5}\pi^{2.5}} \frac{e^6}{\varepsilon_0^3 c^3 m^{1.5}\hbar} Z^2 \frac{\exp\left(-\frac{h\nu}{kT}\right)}{\sqrt{kT}}. \tag{19}$$

The numerical constant in Eq. (19) amounts to 3.00×10^{-6} when using a.u. througout (including for N_e, N_i, and the time), 3.8×10^{-29} when using SI units all throughout, and 3.0×10^{-21} in the same case but for the temperature in keV in the square root.

The integration over E is conveniently calculated in a Maxwellian plasma by the Gauss-Laguerre method [14] with abscissa t_i and weight factors w_i. The Gaunt factor for emissivity coefficients amounts to

$$\frac{J^i(h\nu)}{J_{\mathrm{Kr}}(h\nu)} = \frac{1}{kT}\exp\left(\frac{h\nu}{kT}\right)\int_{h\nu} G^i(E,h\nu)\exp\left(-\frac{E}{kT}\right)dE = \sum_j w_j G^i(t_j kT + h\nu, h\nu). \tag{20}$$

When the Born or EB cross-section Gaunt factors of Eqs. (5), (6), and (8) are used, it is a function of the two dimensionless quantities $h\nu/kT$ and $L_i = 2\sqrt{2mkT}/(\hbar\lambda_i)$. Because of the exponential decrease, the influential Gaunt factors correspond to E close to $h\nu$. Since the Elwert factor has been

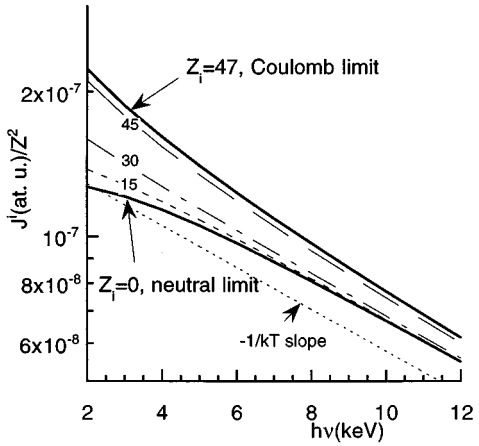

FIG. 14. Emissivity coefficients for Ag ions in a plasma of temperature $T=10$ keV vs photon energy, as obtained in the EB approximation by Eq. (25).

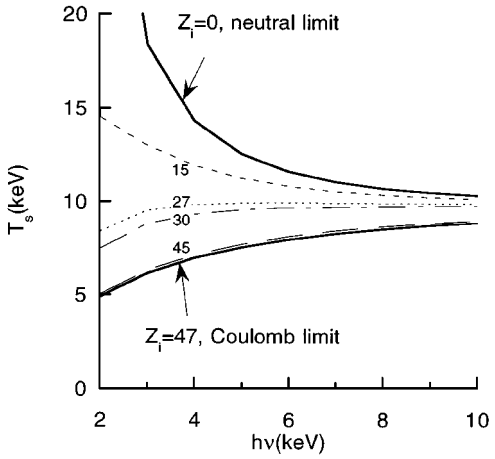

FIG. 15. Spectral temperatures deduced from the emissivity coefficients of Fig. 14 by Eq. (21). Same notations as in Fig. 14.

introduced to improve the quality of the cross sections in that region, J_{EB} will be a better estimate than J_B. This might be the contrary only at high T's, but then the plasma would be fully ionized and estimations for partially ionized atoms would not be needed. On the other hand, in the region of very small $h\nu$'s, the line emission and radiative recombination would dominate the spectrum.

The exponential behavior of J_{Kr} in Eq. (19) implies an obvious temperature diagnostic [3]. When using cross sections more sophisticated than Kramers ones, the ''spectral temperature'' T_s defined below depends on the photon energy at which it is evaluated and may significantly differ from the thermodynamical temperature T. Application of the direct simple diagnostic can then be misleading even in a Maxwellian plasma

$$kT_s=-\frac{d[h\nu]}{d\ \ln[J(h\nu)]}\neq kT,\quad T_{s,\mathrm{Kr}}\equiv T. \tag{21}$$

B. Results of emissivity coefficients

Some $J^i_{\mathrm{EB}}(h\nu)$ results are plotted in Fig. 14 for silver at $T=10$ keV. Though the highly ionized ions are abundant in that plasma, the curves are drawn from $Z_i=0$ to Z in order to show how J/Z^2 depends on Z_i. The emission is larger for the higher Z_i's because the G's are bigger at small $h\nu/E$ when the potential is more Coulombic. The trend is stronger at small $h\nu$'s, since the contribution of the electrons with smaller $h\nu/E$ is then more dominant. Figure 14 shows, in addition, the straight line relative to J_{Kr}/Z^2. The curves corresponding to the small and large Z_i's do not run parallel to it, especially at small $h\nu$'s.

Figure 15 shows the ''spectral temperature'' deduced from the emissivity curves of Fig. 14. Only for $Z_i=27$ is T_s close to T over the whole photon range. For Z_i/Z close to 0 or to 1, T_s significantly differs from T at small $h\nu$'s, as expected. A precise interpretation of experimental spectra would then require some knowledge of the ionic populations and a good estimate of $J(h\nu)$ for the abundant ions.

Values of $J(h\nu)/J_{\mathrm{Kr}}(h\nu)$ are shown in Fig. 16 for the same plasma, for both EB and Born approximations and only for the two limits $Z_i/Z=0$ and 1. The Coulomb and neutral atom results become close to each other at high $h\nu/kT$ in each approximation since the electrons involved become more energetic and the screening effect thereby negligible. As expected from Eq. (20), $J_{\mathrm{EB}}(h\nu)/J_{\mathrm{Kr}}(h\nu)$ goes over to $G_{\mathrm{EB}}(h\nu,h\nu)=1.10$. On the contrary, the screened and the Coulomb results differ from each other at small $h\nu/kT$ where the screening is more influential. At this end of the spectrum the EB and Born approximations lead to similar results because the Elwert factor is close to one for small $h\nu/E$ values.

Figure 16 shows that $F=J_{\mathrm{EB}}/J_B$ increases with $h\nu/kT$ and suggests that this ratio is nearly the same for the neutral and the Coulomb cases. The value of $F(h\nu/kT)$ can be evaluated by using $G_{\mathrm{EB}}(E,h\nu)=a(h\nu)+b(h\nu)\ln(E)$, as suggested by Fig. 8 and Eq. (10). The corresponding Born Gaunt factor is $G_B(E,h\nu)=\sqrt{1-h\nu/E}\ \ [a(h\nu)+b(h\nu)\ln(E)]$. When performing the integration of Eq. (20), we find

$$\frac{J_{\mathrm{EB}}(h\nu)}{J_{\mathrm{Kr}}(h\nu)}=[a(h\nu)+b(h\nu)\ln(h\nu)]-b(h\nu)\times\mathrm{Ei}(-h\nu/kT)\exp(h\nu/kT)=C+D. \tag{22}$$

The second term D involving the exponential integral function E_i is usually smaller. The Born emissivity cannot be obtained analytically and is calculated by the summation in Eq. (20). The part of the integrand that brings in the term C in Eq. (22) for the EB approximation leads to the term C/F_1 in the Born approximation, while the part that brings in the term D leads to D/F_2. At each pole, we define the quantity $y_i=(1/t_i)(h\nu/kT)$. The factors F_1 and F_2 rigorously depend only on the ratio $h\nu/kT$ and amount, respectively, to

$$F=\frac{J_{\mathrm{EB}}}{J_B}\cong F_1(h\nu/kT)=\frac{1}{\sum_i w_i/(1+y_i)}>F_2(h\nu/kT)=\frac{\sum_i w_i\ln(1+1/y_i)}{\sum_i w_i/(1+y_i)\ln(1+1/y_i)}. \tag{23}$$

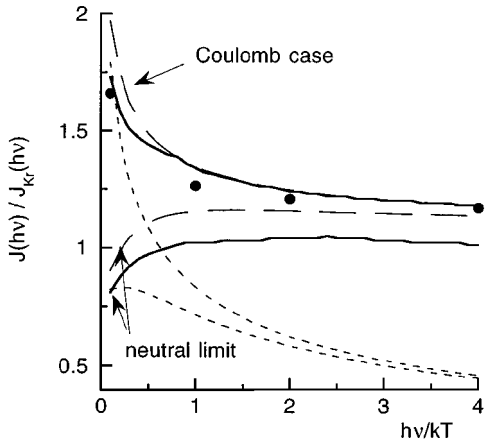

FIG. 16. Ratio J/J_{Kr} for the neutral atom and Coulomb cases vs $h\nu/kT$ for Ag in a plasma at $kT=10$ keV. ---, Born approximation; ––, Elwert-Born approximation; —, using PF [13] cross sections for the Coulomb case and PW elaborate cross sections [5] for the neutral limit; ●, Karzas-Latter results [15].

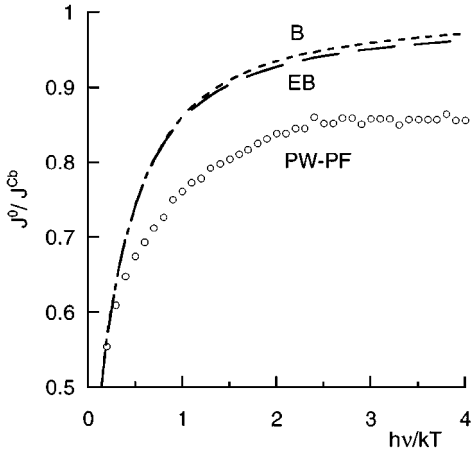

FIG. 18. Ratio of the neutral atom to the Coulombic emissivity coefficient. ---, Born approximation; ––, Elwert-Born approximation; ○, using PF [13] cross sections for the Coulomb case and PW elaborate cross sections [5] for the neutral limit.

These two factors are drawn in Fig. 17. The actual ratios F are expected to be between these two values and much closer to F_1. The numerical results of $J_{\mathrm{EB}}(h\nu)/J_B(h\nu)$ corresponding to the silver plasma at 10 keV for the neutral atom and Coulomb extreme cases are also plotted in the same figure. They are close to each other as well as very close to F_1. We found very similar values of $F(h\nu/kT)$ for partially ionized silver atoms and for higher T's. Whatever the ionic composition of the plasma the EB and Born estimates will thus differ within a precision of a couple of percent by the factor F_1. It is close to 1 and J_B would thus be acceptable only at small $h\nu$'s where the spectrum is dominated by line emission and radiative recombination. In conclusion, J_{EB} is always the proper choice in regions of practical interest.

C. Recommendations for the determination of ionic emissivity coefficients

From the preceding subsection it can be concluded that for any given value of $h\nu/kT$ we have $J^0_{\mathrm{EB}}/J^{\mathrm{Cb}}_{\mathrm{EB}}=J^0_B/J^{\mathrm{Cb}}_B$ and this is indeed verified for the silver example (see Fig. 18). It would be tempting to conclude that this ratio is accurate, as was verified for the energy losses $W(E)$ in Sec. III. Such a step is not obvious because of a complete lack of J_{PW} published results, both in the Coulomb and in the neutral atom cases. In the Coulomb case, we cannot even calculate the $J^{\mathrm{Cb}}_{\mathrm{PW}}$ because there is nearly no $G^{\mathrm{Cb}}_{\mathrm{PW}}$ published. In order to determine at least a more exact J^{Cb}, we started from the Coulombic Gaunt factors recommended by Pratt and Feng (PF) [13]. The $J^{\mathrm{Cb}}_{\mathrm{PF}}$ curve obtained is shown in Fig. 16. We also plotted a few nonrelativistic quantum-mechanical data, as we could read them approximatively from Figs. 3–5 of the article by Karzas and Latter [15]. For the E energies involved at that temperature, the relativistic effects are negligible and the Karzas-Latter (KL) points should be close to the $J^{\mathrm{Cb}}_{\mathrm{PF}}$ curve. The agreement is indeed observed in Fig. 16, which confirms that we can take the $J^{\mathrm{Cb}}_{\mathrm{PF}}$ curve as a reasonably exact curve. For $h\nu/kT>1$, $J^{\mathrm{Cb}}_{\mathrm{PF}}$ is also very close to these two sets of Coulomb results, as in fact the nonrelativistic EB approximation is valid. Coming now to the determination of J^0_{PW}, we used in the second part of Eq. (20) Gaunt factors doubly interpolated from the PW cross sections tables [5]. The curve $J^0_{\mathrm{PW}}/J_{\mathrm{Kr}}$ is drawn in Fig. 16. It lies below the $J^0_{\mathrm{EB}}/J_{\mathrm{Kr}}$ curve. This was expected since the G^0_{PW} are always smaller than the G^0_{EB} in the region of large $h\nu/E$ (see Figs. 4 and 5). We conclude that

$$\frac{J^0_{\mathrm{EB}}(h\nu)}{J^{\mathrm{Cb}}_{\mathrm{EB}}(h\nu)}\cong\frac{J^0_B(h\nu)}{J^{\mathrm{Cb}}_B(h\nu)}>\frac{J^0_{\mathrm{PW}}(h\nu)}{J^{\mathrm{Cb}}_{\mathrm{PF}}(h\nu)}. \tag{24}$$

This result is illustrated in Fig. 18 for the Ag plasma at 10 keV. Because of the last inequality, it would not bring any improvement to use extrapolation or interpolation laws involving ratios J^0_B/J^i_B or $J^0_{\mathrm{EB}}/J^i_{\mathrm{EB}}$. The precision on the result would in fact not be better than the precision on the direct EB evaluation. The last one is overestimated by the unprecision of G^0_{EB} at the first pole, that is, $G(1.116kT+h\nu,h\nu)$ when using 12 poles. If $h\nu$ is bigger than around 5 keV and $h\nu+3kT$ is smaller than around 200 keV, the precision of J^i_{EB} through Eq. (20) should be better than 12%. In conclu-

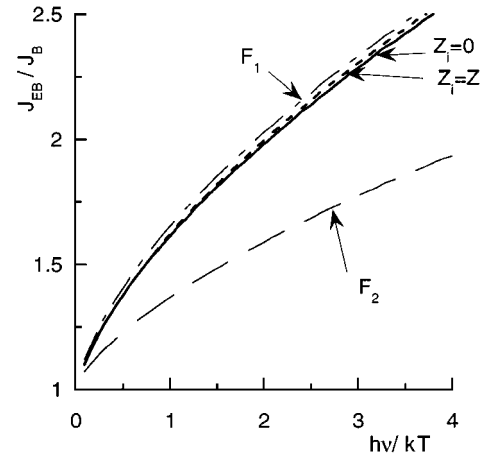

FIG. 17. Ratio of the EB to the Born emissivity coefficient for Ag neutral (—) and Coulomb (---) cases in a plasma of temperature $T=10$ keV, as obtained by Eqs. (20), (6), and (8), compared to the factors F_1 and F_2 of Eq. (23).

sion, unless at high photon energies or temperatures where relativistic Coulomb cross sections should be used, such as the ones of Ref. [23], the emissivity coefficient is given satisfactorily by

$$\frac{J^i_{\rm EB}(h\nu)}{J_{\rm Kr}(h\nu)}=\sum_j w_j G^i_{\rm EB}(t_i kT+h\nu,h\nu), \tag{25}$$

using $G_{\rm EB}$ from Eqs. (6) and (8).

V. TOTAL POWER EMITTED BY A MAXWELLIAN PLASMA

A. Expression of the total power emitted

The total power radiated P ((dimension)=(energy)[(volume)/(time)]) is given equivalently by the integration of $W(E)$ over the electron energy distribution or of $J(h\nu)$ over $h\nu$:

$$P=\int_0^\infty W(E)f(E)v\ dE=\int_0^\infty J(h\nu)d(h\nu). \tag{26}$$

The reference $P_{\rm Kr}$ based on Kramers cross sections is, immediately,

$$P_{\rm Kr}=\frac{1}{2^{1.5}3^{1.5}\pi^{2.5}}\frac{e^6}{\varepsilon_0^3 c^3 m^{1.5}\hbar}Z^2\sqrt{kT}, \tag{27}$$

where the constant is 3×10^{-6} (in a.u.), 3.84×10^{-29} (in SI units), and 4.86×10^{-37} in the second case but for kT in keV. The total power loss off an optically thin plasma is, finally, per unit of volume, $\Sigma_i N_e N_i P^i$.

The dependence of the ionic total power loss on the individual cross-section Gaunt factors is given by a double Gauss Laguerre integration

$$\frac{P^i}{P_{\rm Kr}}=\sum_j w_j t_j\frac{W^i(E=t_jT)}{W_{\rm Kr}}=\sum_j w_j\frac{J^i(h\nu=t_jT)}{J_{\rm Kr}(h\nu=t_jT)}, \tag{28}$$

$$\frac{P^i}{P_{\rm Kr}}=\sum_j w_j\sum_k w_k G^i[E=(t_k+t_j)kT,h\nu=t_jT]. \tag{29}$$

In the Born and EB approximations the $P^i/P_{\rm Kr}$ by use of Eqs. (14) and (15), depend only on $\alpha=Z/Z_i$ and on the dimensionless parameter $L_i=2\sqrt{2mT}/(\hbar\lambda_i)$. When using 12 poles in each summation, 144 cross sections are needed in Eq. (29), but only the j-k pairs with j and $k<6$ are usually contributing significantly. Since the second pole has the biggest weight w, the major contribution comes rigorously from the pair $t_k=t_j=t_2=0.611$ in Kramers approximation and in fact also when using $G^{\rm Cb}_{\rm EB}$. This pair corresponds to $h\nu/E=0.5$. It thus seems essential that the cross section for that point be of a good quality. The contributions leading to more than two-thirds of P come from the much wider region $h\nu/E=t_j/[t_j+t_k]=0.10$–$0.85$. Good cross sections thus seem to be needed over nearly the whole spectrum. The considerations of Sec. III fortunately let us hope for favorable cancellations effects.

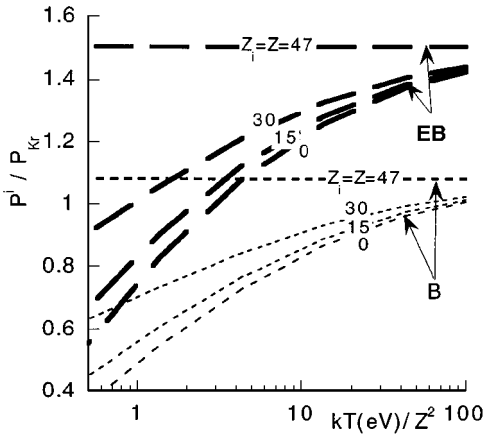

FIG. 19. Total power losses for Ag ions vs kT(eV)/Z^2 as obtained in the Born (---) and EB (––) approximations by Eqs. (28), (14), and (15). Ag plasma at a temperature of 10 keV.

B. Results of total power losses

Results in the Born and EB approximations are given in Fig. 19 for various degrees of ionization. The two sets of values differ by a factor of 1.39–1.54. It is close to the value of the Elwert factor $\sqrt{2}$ for the dominant above pair $i=j=2$ and is consistent with Eq. (16). Of course, P^i is smaller for smaller Z_i and kT.

Results are given in Fig. 20 in the Coulomb case for which Eqs. (13) and (28) straightforwardly lead to

$$\frac{P^{\rm Cb}_B}{P_{\rm Kr}}=\frac{2\sqrt{3}}{\pi},\quad \frac{P^{\rm Cb}_{\rm EB}}{P_{\rm Kr}}=\frac{2\sqrt{3}}{\pi}2\ \ln 2. \tag{30}$$

These two constant values encompass the KL data points obtained in the Sommerfeld approximation, as we read them approximately from Fig. 6 of Ref. [15]. We also determined $P^{\rm Cb}_{\rm PF}$ from the Coulomb cross sections of Ref. [13]. The curve obtained lies in agreement with the KL points only for not

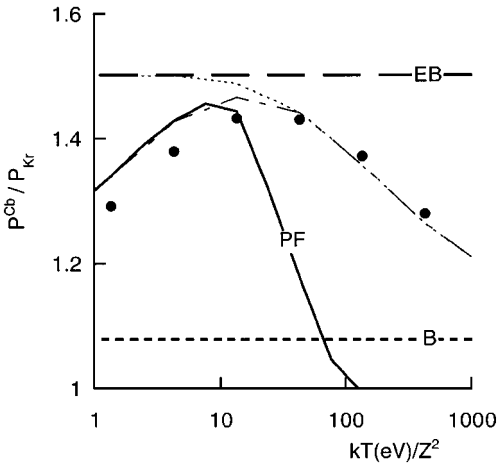

FIG. 20. Total power losses for the Coulomb limit. ---, Born approximation; ––, EB approximation of Eq. (30); ·····, EB approximation but using the full expression of the Elwert factor in Eq. (7); —, based on the Coulomb cross sections of Ref. [13] and Eq. (29); –·–, same as —, but when always imposing nonrelativistic cross sections; ●, Karzas-Latter results [15].

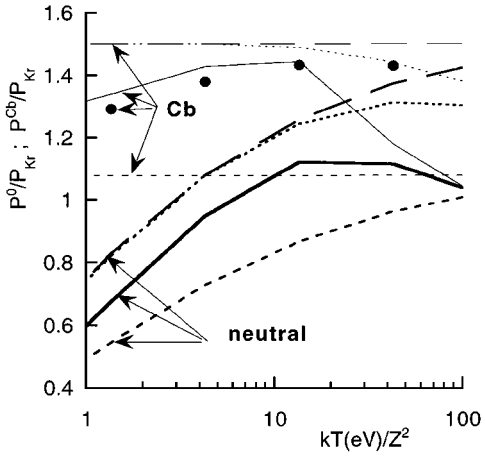

FIG. 21. Total power losses for the Coulomb and neutral limits. Same notations as in Fig. 20, but for the use of the parametric potential in the neutral case (—) obtained from Eq. (29) by use of interpolated elaborate PW cross sections [5].

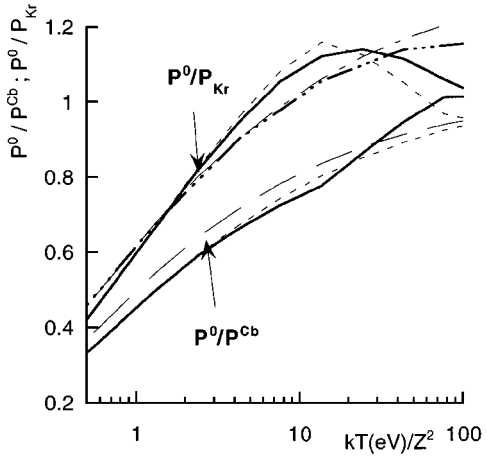

FIG. 22. P^0/P^{Cb} is the ratio of the neutral atom to the Coulombic total power loss: ---, Born approximation; ––, EB approximation; —, using PF [13] cross sections for the Coulomb limit and interpolated elaborate PW cross sections [5] for the neutral limit. P^0/P_{Kr} is the neutral estimate. ----, extrapolated from the P_{PF} by Eq. (31); ––-, based on using $0.5(W^0_{\mathrm{EB}}+W^0_B)$ as in Eq. (32); –···–, same as ––-, but using the full expression of the Elwert-Gaunt factor in W^0_{EB}; –, evaluation from Eq. (29) by interpolating from elaborate PW cross sections [5].

too large T's, as the quantum model of Sommerfeld is nonrelativistic. In Pratt and Feng's, more versatile evaluation, there is an energy domain where Elwert-Born cross sections are used. In that case, the relativistic formula [23] is adopted for heavy ions when $E>(2Z\alpha_{\mathrm{FS}})^4\times 511$ keV$=2.32\times10^{-5}\,Z^4$ keV, that is, 113 keV for $Z=47$. If we impose that the Elwert-Born approximation be always applied in the nonrelativistic form, we indeed reproduce the KL curve over the whole abscissa range considered in Ref. [15], that is, until $kT(\mathrm{eV})/Z^2=13\,600$. Figure 20 also shows that the KL points coincide at large T's with the full Elwert-Born-Coulomb approximation using $\mathcal{E}_F(E,h\nu)$ of Eq. (7). This again shows that the KL data are correct only for small or moderate temperatures.

At very high T's, we also question about our simple estimates. After looking at the exact Coulomb cross sections [5] for $Z=47$ it seems prudent to avoid situations when significant contributions to P come from cross sections involving $E>E_{\mathrm{lim}}=250$ keV, which roughly sets the limit of $T=E_{\mathrm{lim}}/5=50$ keV. It is not restrictive since Ag is already fully stripped at smaller temperatures except for the case of extremely tenuous plasmas. Therefore the figures to come will not cover huge temperatures, unlike what was done in former papers [15,10], where results were given far beyond the domain of validity of the nonrelativistic atomic models used.

As a last remark, we mention that use of the full Elwert factor of Eq. (7) is only slightly more satisfying at large but still reasonable T's than use of the simple Elwert factor. This would make us lose the one parameter L_i dependence mentioned above for the sake of a negligible advantage. In other words, we switch directly from a domain where the nonrelativistic simplified EB approximation in a screened potential is a good approximation to a domain where the full relativistic Coulomb treatment is necessary.

Figure 21 gives results in the two extreme cases $Z_i=Z$ and 0 for the abscissa $kT(\mathrm{eV})/Z^2=1$–100. We checked again that full Elwert-Born and simplified Elwert-Born approximations give the same values at these temperatures of around 50 keV. The Coulomb Pratt-Feng and KL results fall between the Coulomb EB and Born curves. Moreover, we calculated the P^0_{PW}, using again exact W^0_{PW} by interpolations from tables [5]. It lies between the neutral atom Born and EB curves, as expected indeed from the W^0 results of Fig. 10. The energy loss W^0_{EB} was slightly bigger than the more exact W^0_{PW} at small E values and W^0_B was slightly smaller. Owing to the integration over E, the curve for the total power loss lies about halfway between the EB and Born curves until the abscissa of around 50 (i.e., kT of 110 keV), where it merges into the Coulomb curve.

C. Recommendations for the determination of ionic total power losses

As expected from these remarks and from Fig. 21, the ratios of the neutral over the Coulomb total power losses are very similar in the three models used (see Fig. 22) so that we could try to evaluate the total power loss by

$$P^i=P^{\mathrm{Cb}}[P^i/P^{\mathrm{Cb}}]_{B\ \mathrm{or\ EB}}. \tag{31}$$

The precision of the determination lies again in the precision with which exact Coulomb data are known. As the Karzas-Latter results are limited to small T's and are only readable from a few curves, use of the Coulomb cross sections of Ref. [13] seems, at present, to be the only possibility enabling one to cover a large temperature range. They have the drawback of being a succession of four types of evaluations with no smoothing between the four regions of validity and they may not be precise enough, no more than the $W^{\mathrm{Cb}}_{\mathrm{PF}}$ in Table I. Figure 21 confirms indeed that it is just as satisfying to take the median of the EB and Born estimates. The total power loss Gaunt factor for an ion of degree of ionization i is thus easily obtained by

$$\frac{P^i}{P_{\rm Kr}} = \sum_j w_j t_j \frac{W^i\left[P_i = \dfrac{2\sqrt{2mt_jT}}{\hbar\lambda_i}\right]}{W_{\rm Kr}} \tag{32}$$

using Eq. (17b) for W^i. When using 12 poles, the first 5 terms are usually sufficient. Figure 22 shows that this direct evaluation leads to results of a good quality and of a comparable quality as the ones obtained by the interpolation scheme of Eq. (31). This comes about because the inaccuracy corresponding to the EB and Born approximations are smoothed out by the integrations over $h\nu$ and E as well as by the half sum. Though the neutral atom case is of little interest to hot plasmas, it enables one to probe our screened estimates thanks to the availability of the very precise PW energy losses [5]. The precision is around 3% for this example. Notice that for the other extreme, i.e., the Coulomb case, the precision is 10% based on the same simple use of $0.5(W_B + W_{\rm EB})$, leading then to a constant value of $1.32P_{\rm Kr}$. Figures 19 and 22 show finally that $P^i/P_{\rm Kr}$ does not vary strongly with Z_i, nor with T. The essential temperature dependence of P^i comes from $P_{\rm Kr}$ itself in Eq. (27).

For high T's when all ions are fully stripped, the total power loss can be evaluated from Eq. (29) using the relativistic Coulomb-Gaunt factors of Ref. [23]. The limit temperature can be defined by recalling that the dominant ion in a plasma has an ionization potential such that $I = \zeta kT$, ζ being of order 3 for dense plasmas and as high as 10–15 for low-density hot plasmas [27]. We can admit that all ions are fully ionized for twice that temperature. This sets the limit temperature of $kT_{\rm lim}({\rm eV})/Z^2 \cong 25\zeta$ for a complete ionization.

For lower temperatures, the total power loss for an ion in the plasma is obtained for the examples considered here with a precision better than 10% by the simple equations (32) and (17b). Use of Eq. (17a) instead of Eq. (17b) would evidently lead to an even much better precision.

VI. CONCLUSIONS

For moderate energies and temperatures, the bremsstrahlung losses and emissivities of electrons scattered by partially stripped ions cannot be given correctly by a Coulomb treatment in either the Z/r, Z_i/r, or the $(Z-Z_i)/r$ field. We have noticed anyway that very few data of good quality are published for the Coulomb case itself, especially for the cross sections and the energy losses. Moreover, the J and P Coulomb results given in Figs. 15 should be used only when the nonrelativistic regime is valid. This lack of data makes it unadvisable at present to apply interpolation laws involving the Coulomb limit. Let us finally mention that, until excellent Coulomb data are published, reasonably good Coulomb data over a large energy range can be determined from the cross sections recommended by Pratt and Feng [13].

Returning to our main interest in bremsstrahlung at moderate energies, the screening by the bound electrons plays an important role. On the basis of a comparative study of various approaches, we could establish *ab initio* appropriate expressions by using a screened analytical potential and by playing with relatively simple approximations. The present article provides formulas convenient to use for the ionic radiative losses and emissivities [See Eqs. (2), (17), (25), and (32)].

ACKNOWLEDGMENT

We are very grateful to Professor R. H. Pratt for having raised our interest in this field and for very stimulating discussions.

[1] R. W. P. McWhirter and H. P. Summers, in *Applied Atomic Collisions Physics*, edited by C. F. Barnett and M. F. Harrison (Academic, New York, 1984), Vol. 43-2, pp. 51–111.
[2] W. M. Stacey, in *Fusion Plasma Analysis* (Wiley, New York, 1981), Chap. 10.
[3] W. Lochte-Holtgreven, in *Plasma Diagnostics*, edited by W. Lochte-Holtgreven (North-Holland, Amsterdam, 1968), p. 183.
[4] I. H. Hutchinson, *Principles of Plasma Diagnostics* (Cambridge University Press, Cambridge, 1992), Chap. 5.
[5] R. H. Pratt, H. K. Tseng, C. M. Lee, C. MacCallum, and M. Riley, At. Data Nucl. Data Tables **20**, 175 (1977); R. H. Pratt, H. K. Tseng, C. M. Lee, L. Kissel, C. MacCallum, and M. Riley, *ibid*. **26**, 477(E) (1981); L. Kissel, C. MacCallum, and R. H. Pratt, Sandia National Laboratories Reports Nos. SAND81-1377 and SAND81-2517, 1981 (unpublished), available from the DOE/TIC, P.O. Box 62, Oak Ridge, TN 37830.
[6] B. F. Rozsnyai, J. Quant. Spectrosc. Radiat. Transfer **22**, 237 (1979).
[7] I. J. Feng, M. Lamoureux, R. H. Pratt, and H. K. Tseng, Phys. Rev. A **27**, 3209 (1983).
[8] M. Lamoureux, R. Cauble, Longhuan Kim, F. Perrot, and R. H. Pratt, J. Quant. Spectrosc. Radiat. Transfer **37**, 283 (1987).
[9] N. B. Avdonina and R. H. Pratt, J. Quant. Spectrosc. Radiat. Transfer **50**, 349 (1993).
[10] N. B. Avdonina, M. Lamoureux, and R. H. Pratt, Proceedings of the Sixth Conference of the International Radiation Physics Society, Maroc, 1994 [Appl. Radiat. Isot. **46**, 445 (1996)].
[11] Longhuan Kim and R. H. Pratt, Phys. Rev. A **36**, 36 (1987).
[12] C. M. Lee, L. Kissel, R. H. Pratt, and H. K. Tseng, Phys. Rev. A **13**, 1714 (1976); **24**, 2866(E) (1981).
[13] R. H. Pratt and I. J. Feng, in *Atomic Inner-Shell Physics*, edited by B. Craseman (Plenum, New York, 1985), pp. 533–580. [A minus sign should be added to the expression of d_2 in Eq. (12) and 8 should replace 2 in front of E_iE_f in the first term of the second line of Eq. (19).]
[14] *Handbook of Mathematical Functions*, edited by M. Abramowitz and I. Stegun (Dover, New York, 1965), p. 923.
[15] W. J. Karzas and R. Latter, Astrophys. J. Suppl. **6**, 167 (1961).
[16] A. Bechler and R. H. Pratt, Ann. Phys. (N.Y.) **163**, 28 (1985).
[17] D. Botto, J. McEnnan, and R. H. Pratt, Phys. Rev. A **18**, 580 (1978).
[18] D. Bunaciu, V. Florescu, R. H. Pratt, and Young Soon Kim, Nucl. Phys. A **339**, 329 (1980).
[19] D. Botto, University of Pittsburgh Report No. Pitt-243, 1980 (unpublished), reprints available from R. H. Pratt.
[20] D. Liberman, J. T. Waber, and D. T. Cromer, Phys. Rev. A **27**, 137 (1965).

[21] H. K. Tseng and R. H. Pratt, Phys. Rev. A **3**, 100 (1971).
[22] C. M. Lee, R. H. Pratt, and H. K. Tseng, Phys. Rev. A **16**, 2169 (1977).
[23] H. A. Bethe and W. Heitler, Proc. R. Soc. London, Ser. A **146**, 83 (1934), formula recalled in Ref. [13].
[24] I. J. Feng and R. H. Pratt, University of Pittsburgh Report No. Pitt-266, 1981 (unpublished), reprint available from R. H. Pratt.
[25] M. Lamoureux and R. H. Pratt, in *Proceedings of the Second International Conference on the Radiative Properties of Hot Dense Matter, Sarasota, 1983*, edited by J. Davis, C. Hooper, R. Lee, A. Merts, and B. Rozsnyai (World Scientific, Singapore, 1985), p. 241.
[26] M. Lamoureux, Adv. At. Mol. Opt. Phys. **31**, 233 (1993), and references therein.
[27] R. M. More, in *Proceedings of the NATO Advanced Study Institute on Atoms in Unusual Situations*, Vol. 143 of *NATO ASI Series B: Physics*, edited by J. P. Briand (Plenum, New York, 1986), pp. 155–215.